Nano Energy 122 (2024) 109262

Contents lists available at ScienceDirect

Nano Energy

journal homepage: www.elsevier.com/locate/nanoen

Full paper

High-performance radial junction solar cells on ZnO coated stainless steel with excellent flexibility and durability

Shuyi Wang [a], Shaobo Zhang [b,*], Zongguang Liu [b], Junzhuan Wang [a], Jun Xu [a], Linwei Yu [a,*]

[a] School of Electronics Science and Engineering/National Laboratory of Solid State Microstructures/Collaborative Innovation Center of Advanced Microstructures, Nanjing University, 210023 Nanjing, PR China
[b] College of Physical Science and Technology/Microelectronics Industry Research Institute, Yangzhou University, 225009 Yangzhou, PR China

ARTICLE INFO

Keywords:
Radial junction
One-pump-down
ZnO-coated stainless steel
Flexibility

ABSTRACT

High flexibility and industrial compatibility are the key factors for developing large-scale lightweight, wearable, and portable thin film flexible solar cells. Here, a rather flexible and mechanically durable three-dimensional (3D) radial junction (RJ) solar cell has been directly constructed over discrete standing Si nanowires (SiNWs), upon flexible ZnO-coated stainless steel (SS) foil substrates. The ZnO layer deposited on the SS surface can optimize the density of SiNWs to improve the optoelectronic performance. A power conversion efficiency of 6.01% has been accomplished, with open-circuit voltage and photo-current density of 0.76 V and 12.87 mA/cm^2, respectively. Remarkably, the outstanding mechanical stability of these RJ devices has been recorded, which can sustain > 4000 cycles of large bending to a radius of 2.5 mm, with only a 7% efficiency decrease. Note that the one-pump-down fabrication procedure of this 3D nanostructure RJ cells upon flexible ZnO-coated SS substrates is compatible with the industrial-mainstream Roll-to-Roll technology, holding thus a strong promise to establishing a simple and low-cost strategy for high-performance and durable flexible photovoltaics.

1. Introduction

Flexible hydrogenated amorphous silicon (a-Si:H) thin film solar cells have attracted enormous research attention for their broad applications in portable and wearable electronics [1–5], especially as skin-fitting bio-sensors in real-time personalized health monitoring [6–9]. In comparison to other flexible technologies, such as copper indium gallium selenide (CIGS) [10,11], cadmium telluride (CdTe) [12], lead sulfide (PbS) [13,14], organic [15], and perovskite materials [16,17] or ultra-thin crystalline silicon (c-Si) wafers (thinned by chemical etching or exfoliation) [18,19], a-Si:H thin film can be made via a low-cost, industrial-mature, and large-area technology, without using any toxic or heavy-metal elements, and having a good air-stability, good biotoxicity, and skin-comfortability [20,21], which are the best candidate to fabricate bio-friendly and skin-comfortable electronics/optoelectronics [22,23]. Normally, flexible a-Si:H thin film solar cells are directly prepared on the surface of flexible substrates, for example, metal foil or polymer substrates [21,24,25]. However, the a-Si:H multilayer thin films in conventional planar structures are extremely vulnerable to bending strains on flexible substrates, causing large crack damage and quick decline and failure of the device performance [26,27].

To improve the flexibility and mechanical durability, against repetitive bending, a variety of three-dimensional (3D) nanostructures have been built upon the surface of flexible substrates to suppress the stresses inside solar cells under significant bending, such as nanowires [28–30], nano-cones [4,27], nano-holes [31], and so on. However, fabricating these flexible nanostructures usually requires a complicated process, including etching, transferring, and other procedures [4,19,27,28]. Among these nanostructures, Si nanowires (SiNWs) represent one of the most attractive candidates, as they can be readily fabricated via top-down and bottom-up methods [32–35]. The flexible SiNW solar cells, prepared by mask-etching into ultrathin c-Si wafer, rely on a carefully controlled and expensive wafer-thinning and complicated lithography patterning process [36], which is incompatible with the one-pump-down process (without vacuum breaking) for establishing a low-cost Roll-to-Roll production of thin film solar cells. On the other hand, the catalytical growth of standing SiNWs via the vapor-liquid-solid (VLS) process provides an ideal framework for fabricating radially stacked *p-i-n* junction thin film solar cells, particularly for the construction of flexible solar cells [37–39]. This radial junction (RJ) structure possesses a strong light trapping effect, which thus allows the

* Corresponding authors.
E-mail addresses: shaobozhang@yzu.edu.cn (S. Zhang), yulinwei@nju.edu.cn (L. Yu).

https://doi.org/10.1016/j.nanoen.2024.109262
Received 21 October 2023; Received in revised form 23 December 2023; Accepted 3 January 2024
Available online 5 January 2024

use of a very thin absorber layer (<100 nm) to enhance the built-in field, facilitate carrier collection, suppress light-induced-degradation (LID) effect, and tolerate more defective i-layer material [22,39]. However, in the conventional noble-metal-catalyzed VLS process, a high temperature is needed to decompose the precursor gases and activate a straight growth of well-defined slim SiNWs. Also, the noble metal catalyst residues, efficient minority carrier killers in c-Si, are difficult to be removed without breaking the vacuum. Fortunately, the SiNWs can also be grown via a low-melting-point (LMP) metal-catalyzed VLS process in a plasma-enhanced chemical vapor deposition (PECVD) system, as demonstrated in our previous work by using tin (Sn), indium (In), bismuth (Bi), gallium (Ga) or their alloys as catalysts [37,38,40,41]. These LMP catalysts allow a low-temperature growth down to ~350 °C, opening the route for the use of various metal foils as flexible substrates [6,22,23] as in the industrial Roll-to-Roll thin film fabrication process [38,39,42], while the inclusion of LMP metal atoms in c-Si introduce only shallow or neutral levels in the bandgap of Si [43,44].

Though flexible RJ cells have been successfully demonstrated in our group, taking 15 μm thick Al foil as substrate [22,23], the soft Al foils alone, with relatively low mechanical strength and stability [45,46], is still not a strong enough substrate for sustain large number repetitive bending or subject to lasting stretching strain. So, after 300 times convex-up bending to 5 mm, the RJ units upon Al foils quickly lose 30% of their initial power conversion efficiency (PCE) [23]. Therefore, choosing a mechanically strong but flexible foil substrate, with higher rigidity and durability, is critical for reliable production. To this end, ultrathin stainless steel (SS) foils come to be an attractive choice, as it is already an industry-proven Roll-to-Roll substrate material for flexible solar cells [47,48], with a rather low cost, high conductivity, excellent optical reflectivity, as well as outstanding flexibility/self-sustainability even its thickness below < 50 μm. However, a direct fabrication of flexible RJ thin film solar cells upon SS has not been experimentally explored or testified so far.

In this work, we explore the use of industrial-mature SS foil as flexible substrates to fabricate a highly flexible RJ thin film solar cell within the 3D VLS-grown SiNW framework, as shown in Fig. 1a. After adding a ZnO-thin-film barrier layer and optimizing SiNW density, an energy conversion efficiency (η) of 6.01% can be obtained for RJ units fabricated on SS+ZnO substrates (RJ@SS+ZnO), which is ~30% larger than that (4.58%) of RJs directly on the surface of SS substrates (RJ@SS). It is also noteworthy that the η demonstrated in this work is the highest value for radial single junction flexible solar cells. More importantly, outstanding flexibility and mechanical stability have been witnessed even after 4000 times convex-up bending to a small radius of 2.5 mm, with a η decline of only 7%, indicating a viable approach for one-pump-down fabrication of flexible RJ cells.

2. Experiments

2.1. Device fabrication

The fabrication process of the a-Si:H RJ units is schematically illustrated in Fig. 1b-f. First, the 50 μm thick SS foil substrates were cleaned by ultrasonication in acetone, ethanol, and deionized water, as presented in Fig. 1b. Then, as shown in Fig. 1c, a ZnO thin-film layer with a nominal thickness of ~90 nm was deposited on the surface of the cleaned SS foil (Fig. 1g, showing a rather rough surface) by using magnetron sputtering at room temperature, to form ZnO deposited SS substrates (SS+ZnO), as presented in Fig. 1h. Next, a thin Sn layer (8 nm/4 nm) was thermal evaporated on the surface of SS+ZnO substrate, and then treated by hydrogen (H_2) plasma in the chamber of a PECVD system, with substrate temperature, flow rate, RF power density, and chamber pressure of 200 °C, 20 standard cubic centimeter per minute (SCCM), 10 mW/cm^2, and 30 Pa, respectively, for 5 min, as shown in Fig. 1d, to form discrete Sn droplets as catalyst to mediate the growth of SiNWs. During the 15 min VLS process of p-type SiNWs, a mixture of 60 SCCM H_2, 6 SCCM silane (SiH_4), and 1.8 SCCM diborane dopant (B_2H_6) was introduced as precursor gases, with substrate temperature, RF power density, and chamber pressure of 350 °C, 20 mW/cm^2, and 100 Pa, respectively, as shown in Fig. 1e. After that, an intrinsic a-Si:H layer with thickness of < 100 nm was deposited upon the p-SiNWs, by a plasma of 20 SCCM H_2 and 6 SCCM SiH_4 at 150 °C for 60 min, followed by the coating of an n-type a-Si:H layer with a thickness of ~10 nm, by using 2.3 SCCM phosphine (PH_3) gas as dopant, as presented in Fig. 1i. Finally, the ITO layer was deposited by sputtering through shadow masks to serve as the top transparent electrode, allowing the incident light from the top of RJ units, as shown in Fig. 1j. The final-fabricated RJ@SS+ZnO units with a radially stacked

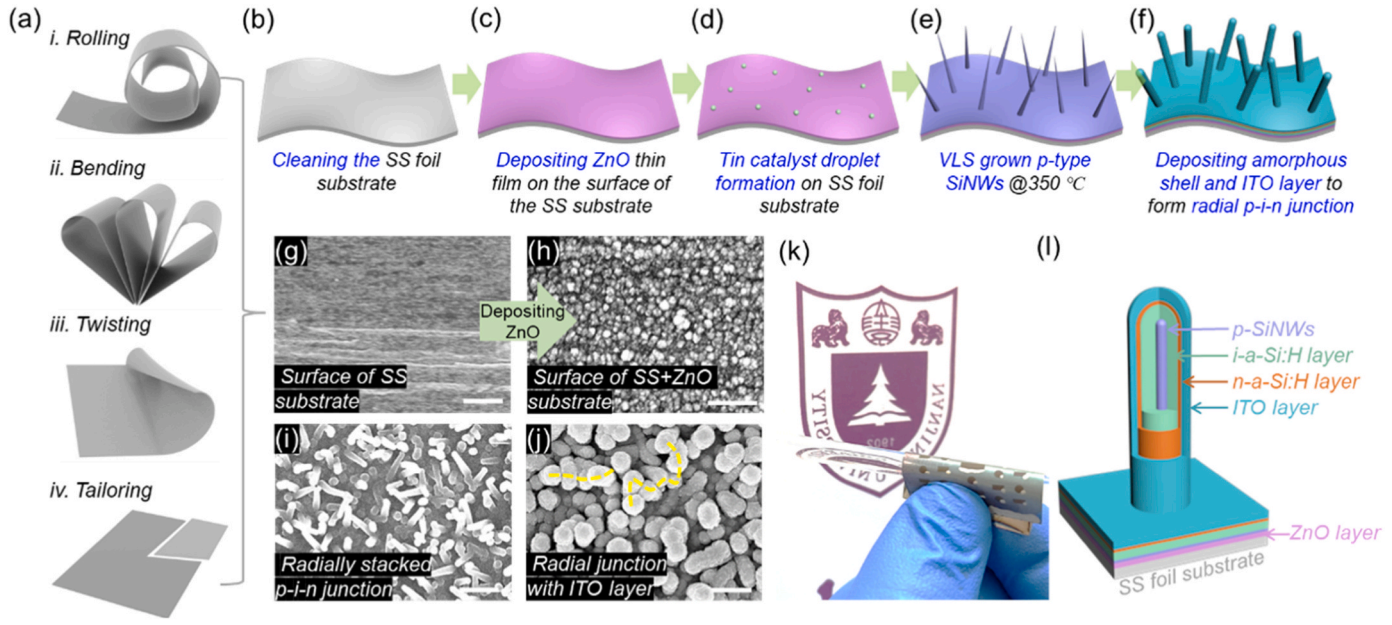

Fig. 1. (a) Sketch map of potential application scenarios (rolling, bending, twisting, and tailoring) of flexible SS foil. (b-f) Schematic illustration of the fabrication procedures of RJ@SS+ZnO units. SEM images of (g) SS substrate, (h) SS+ZnO substrate, (i) RJs without ITO coating, and (j) RJ units coated with ITO layer. (k) Photograph of RJ@SS+ZnO solar cells under 2.5-mm-radius convex-up bending. (l) Schematical diagram of final-fabricated RJ@SS+ZnO. All scale bars are 1 μm.

multilayer structure is schematically illustrated in Fig. 1l. Besides, to provide more details to prove such radially stacked *p-i-n* junction structure, the cross-section of RJ was exposed by using a nano-manipulator to break the selected RJ unit, as shown in Fig. S1d, as well as the SEM images of single p-type SiNW, single RJ unit without/with ITO layer in Fig. S1a-S1c. As seen in the SEM image of the cross-section of the RJ unit, the SiNW can be clearly observed, as well as the deposited amorphous shell and ITO layer around it. More details of the Sn-mediated VLS process of p-type SiNWs in a PECVD system have been carefully described in our previous works [49–52].

2.2. Device characterization

The morphology of the RJ@SS and RJ@SS+ZnO units and reference samples was characterized by scanning electron microscopy (SEM, Zeiss Sigma). The photocurrent density-voltage (*J-V*) measurements of RJ@SS+ZnO units and reference samples were conducted under standard AM 1.5 G illumination conditions (Newport, Oriel Sol-1A, power intensity is 100 mW/cm^2) at room temperature, as well as the corresponding samples after convex-up bending. Normally, there are 17 circle cells with a 1.5 mm diameter, 14 rectangle cells with a 2 mm × 1 mm size, and 3 rectangle cells with a 4.2 mm × 1.6 mm size on a 2.5 cm × 2.5 cm substrate. Besides, as shown in Fig. 1k, for good contact between the electrode and the top ITO layer in *J-V* measurement, tiny Ag dots are usually placed at the edge of ITO regions, usually half in the ITO region and half outside the ITO region. The external quantum efficiency (EQE) curves were measured with a calibrated silicon detector by the QEX-10 system within a wavelength range from 300 nm to 750 nm, and a sweep step of 10 nm, using the rectangle sub-cells with a 4 mm × 1.5 mm size as measured region. The light absorption curves of the fabricated RJ cells were measured by using a UV-Vis-NIR Spectrophotometer (UV-3600 Plus, Shimadzu), ranging from 300 nm to 750 nm with a sweep step of 2 nm. The contact angle measurements were carried out by a sessile drop method via a contact-angle meter (Dataphysics, OCA20), using 1 μL water droplets as examples.

3. Results and discussion

Fig. 1k shows a photograph of the flexible RJ@SS+ZnO solar cells under a 2.5-mm-radius convex-up bending condition, without any encapsulation, package, or attachment to polymer substrates, and a typical side-view SEM image of the RJ structure built on ZnO coated SS is shown in Fig. S1e, where the vertical standing RJ units are somehow randomly oriented and even mutually crossed. The firmly standing SiNW on the surface of substrates can host/support the out-of-plane RJ portions that can be well protected and separated from the strain-rich and unstable bottom regions. Furthermore, as shown in Fig. 1j, this morphology and distribution feature can provide extra current paths, that is the top ITO-crossing pathway (yellow dash line in Fig. 1j), helping to transport and collect the photo-current among the crossed RJs, without the need to go through the more resistive bottom ITO-crossing routes, as reported in our previous work [6,23]. The larger the density of the RJ matrix, the more existence of such an extra top ITO-crossing pathway happens, which can indeed help to overcome the detrimental effect of the cracks induced by flexible substrate bending. Thus, a dense RJ matrix should be more beneficial for better flexibility and mechanical stability. To achieve an optimized density of RJ units, adjusting the thickness of the Sn layer is the best/simplest method, which has been well-established [53]. As in Fig. 2d, when an 8-nm-thick Sn layer is directly evaporated onto the surface of SS substrates as catalysts, the RJ density with a value of 2.25 × 10^8 cm^{-2} can be obtained, however, which is much lower than that achieved on the Al-doped ZnO (AZO) glass substrate in our previous work [39]. After analogizing with the normally used AZO glass substrates, depositing a ZnO-thin-film layer on the surface of SS substrates is considered necessary. Consequently, an obvious improvement of RJ density is observed on the ZnO-deposited SS substrate (SS+ZnO), changing from 2.25 × 10^8 cm^{-2} to 4.53 × 10^8 cm^{-2}, which are extracted from the top-view SEM images of RJ units

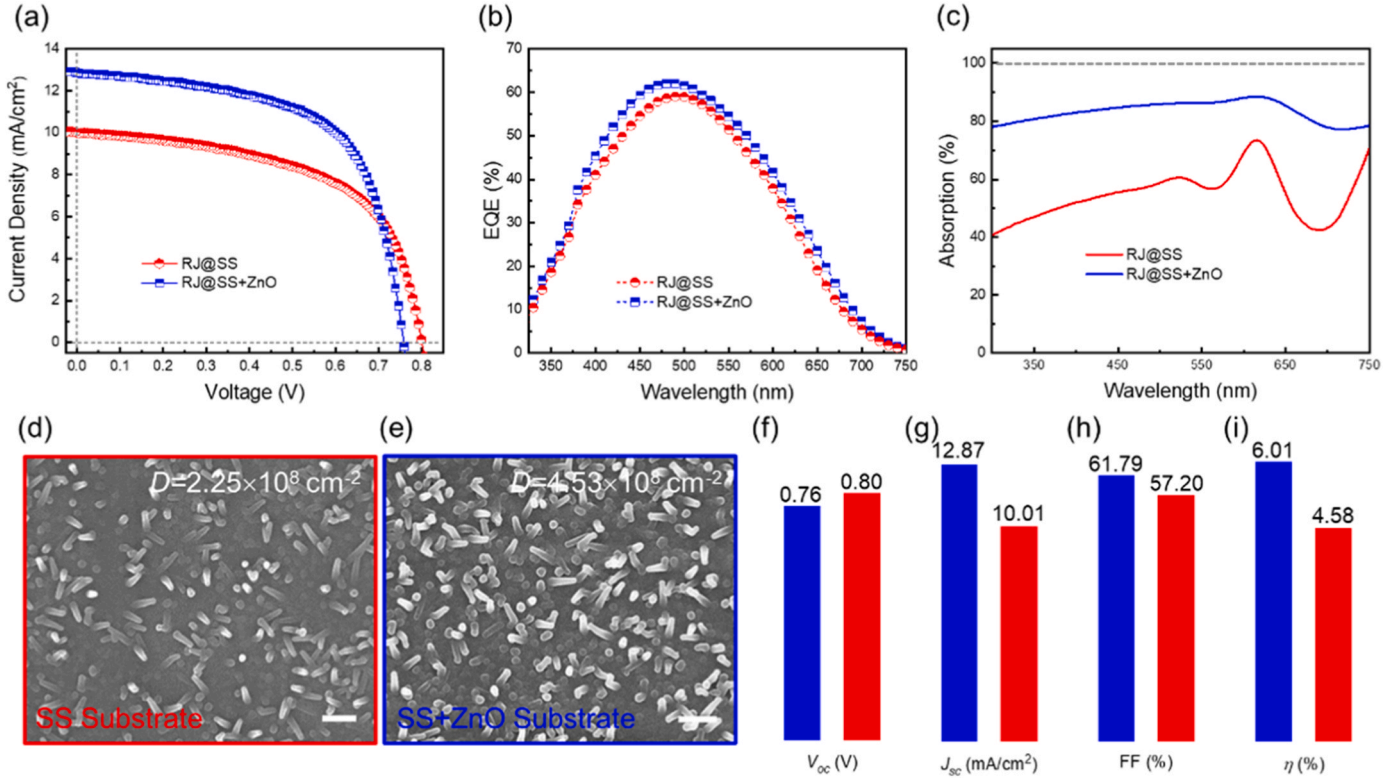

Fig. 2. (a) *J-V* curves (b) EQE curves, and (c) absorption curves of RJ@SS and RJ@SS+ZnO solar cells. SEM images of (d) RJ@SS and (e) RJ@SS+ZnO units. Corresponding photovoltaic performance parameters (f)V_{oc}, (g) J_{sc}, (h) *FF*, and (i) η are extracted and compared in the histograms. Both scale bars are 1 μm.

fabricated on SS and SS+ZnO substrates, as shown in Fig. 2d and e, respectively. Expectedly, a similar phenomenon can also be observed on the density change, when the Sn layer thickness is 4 nm, as shown in Fig. S2a and b.

The *J-V* curves measured under standard AM 1.5 G illumination and the external quantum efficiency (EQE) curves for the RJ@SS+ZnO and RJ@SS units are shown in Fig. 2a and b, as well as the corresponding open-circuit voltage (V_{oc}), short-circuit current density (J_{sc}), filling factor (*FF*), and η are extracted and plotted as column charts shown in Fig. 2f-i, respectively. Note that, thanks to a stronger light trapping effect among the denser RJ matrix (Fig. 2c), a higher J_{sc} of 12.87 mA/cm^2 has been achieved for the RJ@SS+ZnO units, compared to that (10.01 mA/cm^2) of RJ@SS units. A similar trend is observed for the *FF*, which has a value of 61.79% for RJ@SS+ZnO units (Fig. 2h), where the deposited ZnO thin film can act as a barrier layer to prevent metal diffusion from the bottom substrate into the *p-i-n* junctions [54,55]. As to V_{oc} variation, shown in Fig. 2f, RJ@SS+ZnO units have a slightly lower V_{oc} of 0.76 V, which is 0.04 V smaller than one (0.80 V) achieved directly on the SS substrates, which can be assigned to the problem of conformal coating of amorphous shell over a dense SiNW array. After depositing the ZnO layer and fine-tuning the RJ density, the RJ@SS+ZnO units can achieve an overall conversion efficiency of $\eta = 6.01\%$, which largely outperforms RJ@SS units (η of 4.58%) fabricated in the same batch. Meanwhile, the average value of efficiencies measured from 17 sub-cells on one substrate has been plotted along with the standard deviations in Fig. S3d, as well as the average values of V_{oc}, J_{sc}, and *FF* in Fig. S3a-c, respectively, indicating a uniform efficiency distribution, as well as a reasonable reproducibility.

The flexibility of the RJs@SS+ZnO was tested by attaching them to cylinder rods with different radii, ranging from R= 25 mm to 2.5 mm, while the optoelectronic properties are measured after releasing from bending, as schematically illustrated in Fig. 3a-3c, and the photographs of different bending radius are shown in the Fig. S4a-d, respectively. Note that, all the tested samples are not encapsulated by polymer or attached to plastic substrates. It is found that the conversion efficiency of the RJ@SS+ZnO solar cells experiences only a small ~1.0% efficiency drop even after convex-up bending to a 2.5 mm radius. Remarkably, the RJs@SS+ZnO can demonstrate excellent flexibility/mechanical stability that can retain 93% of initial η, 94% of initial V_{oc}, and 98% of initial J_{sc}, even after 4000 times convex-up bending to a very small radius of 2.5 mm, as shown in Fig. 3e, S4e and S4f, measured for the samples fabricated in the same batch. In addition, the planar junction (PJ) units on the ZnO-deposited SS substrates (PJ@SS+ZnO) and RJ@SS units have been fabricated as the references, with their tested flexible properties also presented in Fig. 3e and Fig. S4g-j. However, the performance of PJ@SS+ZnO units shows an 18.5% decline just after 1000 bending cycles with a radius of 2.5 mm, accomplished with a V_{oc} decline of ~3%, and a J_{sc} decline of ~18%, as shown in Fig. S4i and j, respectively. As to the RJ@SS solar cell, it experiences a η decline of ~5% after 2200 bending cycles with a convex-up bending radius of 2.5 mm. Compared to the flexible RJ solar cells that are fabricated directly on the Al foil substrates (just having 71% of initial efficiency after 300 times convex-up with a radius of 5 mm) [23], the ~7% efficiency drop of RJ@SS+ZnO after 4000 times bending with a very small radius of 2.5 mm demonstrates excellent flexibility, which has never been reported for such RJ-structured flexible a-Si:H thin film solar cells.

To have a deep understanding of the flexibility of RJ@SS+ZnO, RJ@SS, and PJ@SS+ZnO units, the surfaces of these samples are examined by SEM after bending of substrates, and shown in Fig. 4 and S5-S7. It is found that several large cracks and peeling-off appear on the surface of the PJ units, as shown in Fig. 4a and S5. While, no matter whether RJ@SS or RJ@SS+ZnO units, which are supported by the VLS-grown SiNWs, are found to be rather continuous and uniform, as shown in Figs. 4d and S6a. The firmly-standing SiNW framework, directly grown on the surface of substrates via a Sn-mediated VLS process, can serve as firmly anchor sites to host the subsequently deposited amorphous shell, thus which can be well protected from stress-rich substrate surface. Also, the randomly distributed RJ units can prevent the

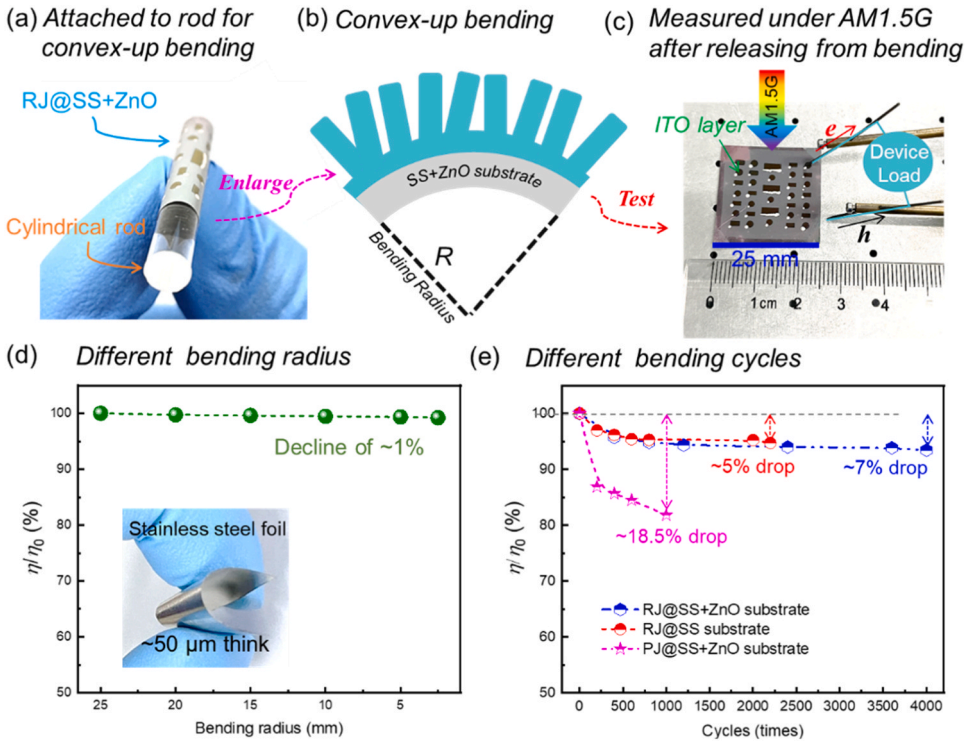

Fig. 3. Bending test conditions of RJs, (a) photo of RJs under bending, (b) sketch map of convex-up bending, (c) photo of measuring after bending. (d) Relative efficiency as a function of different bending radii, and the inset photo: 50 μm thick SS foil used in this work. (e) Relative efficiency of RJ@SS+ZnO, RJ@SS, and PJ@SS+ZnO as a function of bending cycles with a radius of 2.5 mm.

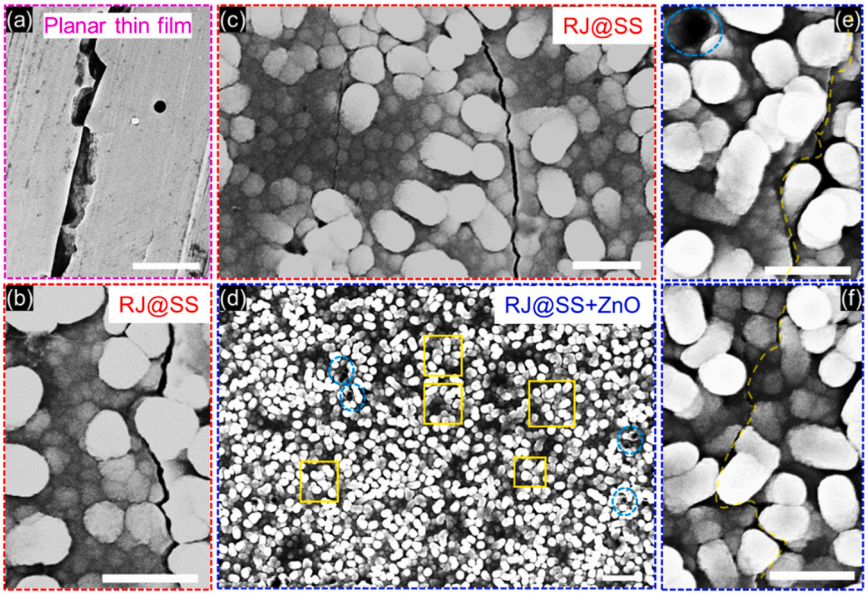

Fig. 4. SEM images of (a) PJ@SS+ZnO, (b, c) RJ@SS, and (d-f) RJ@SS+ZnO after bending. Cracks induced by bending are marked by the yellow square, and cutting-off RJs are marked by blue dash circles. The scale bar in (a) is 10 μm, in (d) is 2 μm, and others are 1 μm.

unlimited or unidirectional crack spreading to some extent, limiting that the cracks just spread on the ground surface of planar regions among the neighboring RJ units, as shown in Figs. 4b, c, and S6. As to the SEM images of the surface of RJ@SS+ZnO units shown in Fig. 4d, there are just some very short and very tiny cracks lying between RJ units, as marked by the dashed yellow line presented in Figs. 4e, f, and S7. It should be noted that a ZnO-thin-film layer has been directly deposited on the surface of SS substrates, where large cracks or peeling-off should appear after 4000 cycles of convex-up bending with a 2.5 mm radius, however, it is not, which is an interesting phenomenon.

Finite element simulations of the PJ@SS+ZnO, RJ@SS, and RJ@SS+ZnO units have also been carried out to shed light on the von Mises stress distribution induced by convex-up bending among the 3D RJ structures. As shown in Fig. S11, the convex-up bending in all simulation models is produced by fixing one edge of the thin SS sheet, and pushing another edge at a certain distance. The von Mises stresses at the surface of SS (red), surface of ZnO thin film (green), surface of Si thin film/root of RJ (blue), middle of RJ (orange), and top of RJ (pink) places, as marked in Fig. 5a, c, and e, are extracted in Fig. 5b, d, f, and corresponding curves are plotted against the tensile strain (caused by a convex-up bending) in Figs. 5g-5i, respectively. As shown in Figs. S11c and 5g, the stress at the surface of ZnO thin film is slightly larger than that extracted at the surface of SS substrates when under a large bending, which can also be observed for RJ@SS+ZnO units, as shown in Figs. 5i and S11i. This simulation is built on the assumption that all surfaces are flat and smooth, however, the realistic surface of SS is rather rough (Fig. 1g), resulting in subsequently deposited ZnO thin film rough, as shown in Figs. 1h and S9a. Such irregularly distributed pyramids can act as a role like texturing to prevent large cracks.

In addition, as shown in Fig. S10, a larger contact angle between droplets and surface, measured by using a water droplet as an example, has been observed on the surface of the ZnO+SS substrates, which can be partially assigned to increased roughness of ZnO+SS substrates [56, 57], in comparison with the SS substrates. Therefore, the Sn layers with the same thickness, on SS and SS+ZnO substrates, will have different droplet distributions after the H_2 deal, resulting in different densities of RJ units. Traces of this situation can be discerned in the SEM images of RJ@SS+ZnO solar cells, as shown in Fig. S9b-e, where among the well-developed long RJ units, there are lots of short stump structures, which are probably the buried short SiNWs catalyzed by the more densely distributed Sn droplets, however, as to RJ@SS, the number of short stump structures among the well-developed long RJ units decreases. In comparison with planar regions among RJ@SS units (as shown in Fig. 4c, where obvious bending-induced cracks spread on the ground surface), such dense short stump structures can also prevent the formation of long and continuous cracks and separate the cracks into local and tiny ones. However, under a large bending, an RJ matrix with a large density will force the nearby RJ units to lean to their neighbors, especially among a local dense RJ “shrubbery”, which may cause some well-developed long RJ to be cut off, as marked by blue dash circles shown in Figs. 4d, e and S8, worsening device performance to some degree. All the above-mentioned unique/interesting features combined contribute to the excellent flexibility and mechanical stability of the RJ@SS+ZnO structure, thus allowing a very small area of cutting, as shown in Fig. S12. The bending, rolling, and twisting caused by cutting with using the scissors have insignificant effect on the performance of RJ@SS+ZnO solar cells.

Compared to other flexible Si-based thin film solar cells that have been reported in the literature and summarized in Table 1, the RJ@SS+ZnO solar cells can spare extra texturing shapes or nanostructures on substrates, and back Ag reflectors. A ~7% decline in efficiency after 4000 times convex-up bending with a small radius of 2.5 mm shows the excellent mechanical stability of this RJ@SS+ZnO technology. More importantly, such RJ@SS+ZnO technology can be fabricated via a one-pump-down process, showing promising potential for establishing a simplest/easiest strategy compatible with industrial-mature Roll-to-Roll technology for a large-area/mass production.

4. Conclusion

In summary, highly flexible and mechanically stable RJ thin film solar cells have been successfully fabricated over the VLS-grown SiNW framework, using ZnO thin film deposited SS foil as flexible substrates. Excellent flexibility and high efficiency (6.01%) have been witnessed by optimizing RJ density and adding a ZnO barrier layer, where RJ@SS+ZnO solar cells are directly constructed upon the rough surfaces of ZnO thin film deposited SS substrates. Even after 4000 cycles of convex-up bending with a small radius of 2.5 mm, the efficiency just shows a ~7% drop. More importantly, such ZnO thin film deposited SS substrates can be well compatible with the industrial-mature Roll-to-

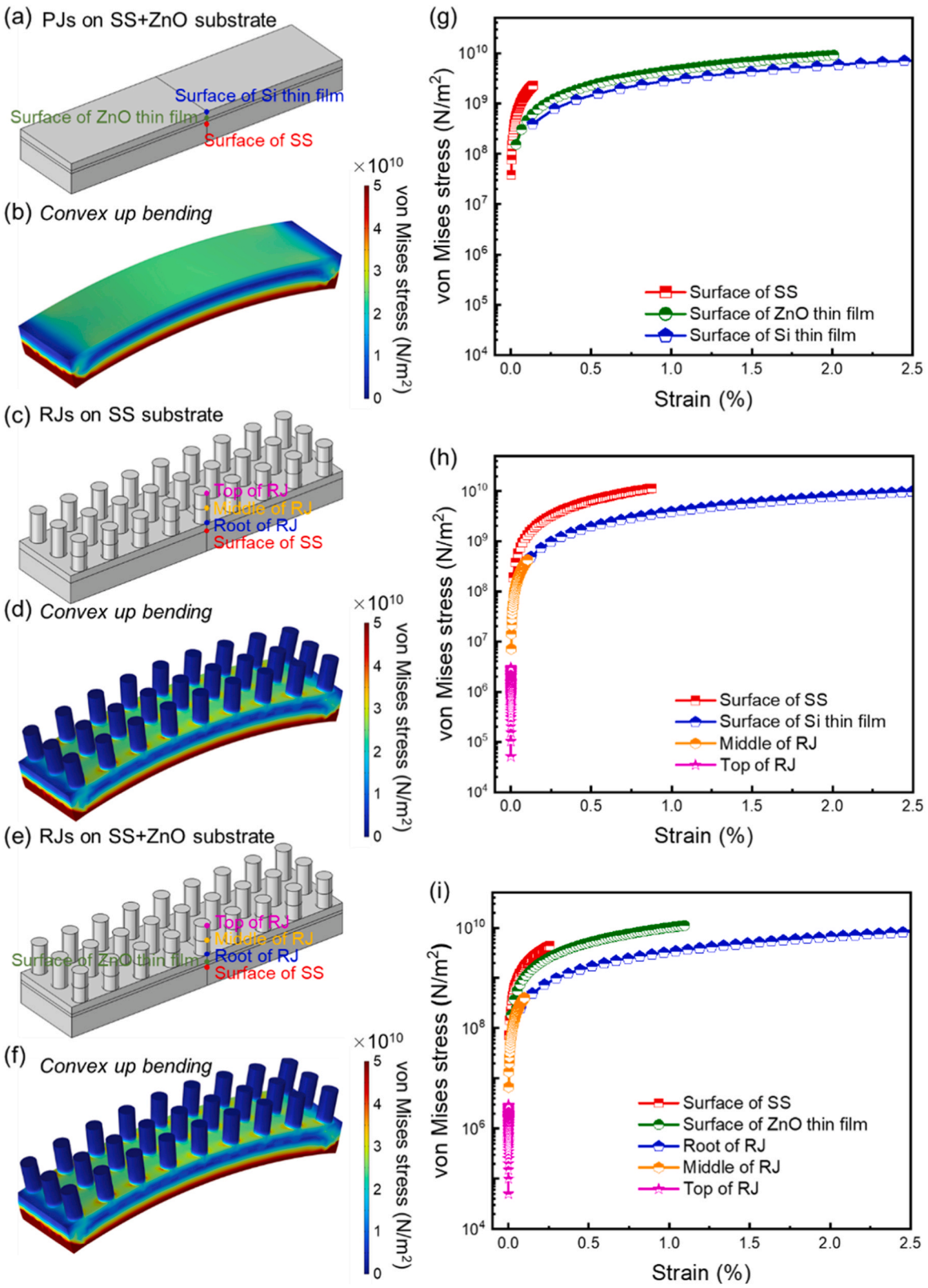

Fig. 5. (a-f) Simulated von Mises stress extracted locations and distribution for PJ@SS+ZnO, RJ@SS, and RJ@SS+ZnO substrates. (g-i) Evolutions of stresses at different extracted locations with different bending strains.

Roll technology for large-area production. These results highlight a promising strategy to establish high-performance flexible photovoltaics technology that can be fabricated via a one-pump-down process compatible with industrial-mainstream PECVD deposition technique, catering to the booming needs of high flexibility, robustness, and low cost in the portable and wearable electronics marketplace.

Table 1
Comparison of this work to other flexible Si-based thin film solar cells in published literature.

Material	*Substrates/Texture/Encapsulation*	*η (%)*	*Bending R*	*Cycles*	*Decline of η (%)*	*Ref.*
n-i-p a-Si:H layers	Graphene papers/PDMS	5.86%	14 mm	100	8%	[5]
p-a-SiC/*i*-a-Si/*n*-a-Si	Parylene template/SiN_x/SiO_x/AZO	5.78%	10 mm	5000	~15%	[21]
n-i-p a-Si:H layers	Nanotextured Ti substrate/Ag back-reflection/AZO	7.26%	2.5 cm	10,000	~3%	[1]
p^+-nc-Si/p^+-a-Si:H/*i*-a-Si:H/n^+-a-Si:H	PEN/SiO_xN_y/AZO	4.93%	14 mm	~350	~70%	[26]
n-a-Si:H/*i*-a-Si:H/PEDOT:PSS	Ag-coated polyimide/TCO	6.52%	1 mm	1	22%	[2]
Radially stacked *p-i-n* multilayers	15 μm thick Al foil	5.6%	5 mm (convex-up)	300	29%	[23]
Radially stacked *p-i-n* multilayers	15 μm thick Al foil/standard EVA polymer encapsulation	5.6%	20 mm (curvature-down)	200	20%	[22]
Radially stacked *p-i-n* multilayers	50 μm thick stales steel	6.0%	2.5 mm	4000	7%	*ours*

CRediT authorship contribution statement

YU Linwei: Conceptualization, Data curation, Formal analysis, Funding acquisition, Investigation, Methodology, Project administration, Resources, Software, Supervision, Writing – original draft, Writing – review & editing. **Zhang Shaobo:** Conceptualization, Data curation, Formal analysis, Investigation, Methodology, Visualization, Writing – original draft, Writing – review & editing. **Liu Zongguang:** Data curation, Formal analysis. **Wang Junzhuan:** Resources, Software, Writing – review & editing. **Xu Jun:** Resources, Writing – review & editing. **Wang Shuyi:** Conceptualization, Data curation, Formal analysis, Investigation, Methodology, Software, Visualization, Writing – original draft.

Declaration of Competing Interest

The authors declare that they have no known competing financial interests or personal relationships that could have appeared to influence the work reported in this paper.

Data availability

Data will be made available on request.

Acknowledgements

The authors acknowledged the financial supports from the National Key Research Program of China under Grant No. 92164201, National Natural Science Foundation of China for Distinguished Young Scholars No. 62325403 and Innovation technology platform project jointly built by Yangzhou City and Yangzhou University (No. YZ2020268).

Appendix A. Supporting information

Supplementary data associated with this article can be found in the online version at doi:10.1016/j.nanoen.2024.109262.

References

[1] S. Cao, D. Yu, Y. Lin, C. Zhang, L. Lu, M. Yin, X. Zhu, X. Chen, D. Li, ACS Appl. Mater. Inter. 12 (2020) 26184–26192.
[2] Y.J. Lee, C. Yeon, J.W. Lim, S.J. Yun, Sol. Energy 163 (2018) 398–404.
[3] Y. Lin, Z. Xu, D. Yu, L. Lu, M. Yin, M.M. Tavakoli, X. Chen, Y. Hao, Z. Fan, Y. Cui, D. Li, ACS Appl. Mater. Inter. 8 (2016) 10929–10936.
[4] C. Zhang, Y. Song, M. Wang, M. Yin, X. Zhu, L. Tian, H. Wang, X. Chen, Z. Fan, L. Lu, D. Li, Adv. Funct. Mater. 27 (2017) 1604720.
[5] X. Zhang, C. Zhang, D. Li, S. Cao, M. Yin, P. Wang, G. Ding, L. Yang, J. Cheng, L. Lu, Nanoscale Res. Lett. 14 (2019) 324.
[6] S. Zhang, T. Zhang, Z. Liu, J. Wang, J. Xu, K. Chen, L. Yu, Adv. Funct. Mater. 32 (2022) 2107040.
[7] T. Zhang, L. Cao, S. Zhang, Z. Liu, J. Wang, Y. Shi, J. Xu, K. Chen, L. Yu, Nano Futures 4 (2020) 035007.
[8] F. Yang, J. Wang, J. Lu, Z. Yu, L. Yu, J. Xu, Y. Shi, K. Chen, P. Roca i Cabarrocas, Adv. Opt. Mater. 5 (2017) 1700390.
[9] Z. Liu, B. Wen, L. Cao, S. Zhang, Y. Lei, G. Zhao, L. Chen, J. Wang, Y. Shi, J. Xu, X. Pan, L. Yu, Adv. Healthc. Mater. 9 (2020) 1901342.
[10] C. Zhang, T. Qi, W. Wang, C. Zhao, S. Xu, M. Ma, Y. Feng, W. Li, M. Chen, C. Yang, W. Li, Sol. Energy 230 (2021) 1033–1039.
[11] K. Ahn, S.-Y. Kim, S. Kim, D.-H. Son, S.-H. Kim, S. Kim, J. Kim, S.-J. Sung, D.-H. Kim, J.-K. Kang, J. Mater. Chem. A 7 (2019) 24891–24899.
[12] W.O. Seo, D. Kim, J. Kim, Opt. Express 23 (2015) A316–A321.
[13] A. Shultz, B. Liu, M. Gong, M. Alamri, M. Walsh, R.C. Schmitz, J.Z. Wu, ACS Appl. Nano Mater. 5 (2022) 16896–16905.
[14] M.M. Tavakoli, M.H. Gharahcheshmeh, N. Moody, M.G. Bawendi, K.K. Gleason, J. Kong, Adv. Mater. Inter. 7 (2020) 2000498.
[15] K. Fukuda, K. Yu, T. Someya, Adv. Energy Mater. 10 (2020) 2000765.
[16] M. Park, H.J. Kim, I. Jeong, J. Lee, H. Lee, H.J. Son, D.E. Kim, M.J. Ko, Adv. Energy Mater. 5 (2015) 1501406.
[17] Q. Luo, H. Ma, F. Hao, Q. Hou, J. Ren, L. Wu, Z. Yao, Y. Zhou, N. Wang, K. Jiang, H. Lin, Z. Guo, Adv. Funct. Mater. 27 (2017) 1703068.
[18] A.B. Roy, S. Das, A. Kundu, C. Banerjee, N. Mukherjee, Phys. Chem. Chem. Phys. 19 (2017) 12838–12844.
[19] J. He, P. Gao, M. Liao, X. Yang, Z. Ying, S. Zhou, J. Ye, Y. Cui, ACS Nano 9 (2015) 6522–6531.
[20] M. Yano, K. Suzuki, K. nakatani, H. Okaniwa, Thin Solid Films 146 (1987) 75–81.
[21] S.-Y. Lo, D.-S. Wuu, C.-H. Chang, C.-C. Wang, S.-Y. Lien, R.-H. Horng, IEEE T. Electron. Dev. 58 (2011) 1433–1439.
[22] S. Zhang, T. Zhang, Z. Liu, J. Wang, L. Yu, J. Xu, K. Chen, P. Roca i Cabarrocas, Nano Energy 86 (2021) 106121.
[23] X. Sun, T. Zhang, J. Wang, F. Yang, L. Xu, J. Xu, Y. Shi, K. Chen, P. Roca i Cabarrocas, L. Yu, Nano Energy 53 (2018) 83–90.
[24] M. Ito, A. Kamath, J. Soc. Inf. Disp. 30 (2022) 309–318.
[25] X. Li, P. Li, Z. Wu, D. Luo, H.-Y. Yu, Z.-H. Lu, Mater. Rep.: Energy 1 (2021) 100001.
[26] R. Yang, C.-H. Lee, B. Cui, A. Sazonov, Mat. Sci. Eng. B 229 (2018) 1–5.
[27] Q. Lin, L. Lu, M.M. Tavakoli, C. Zhang, G.C. Lui, Z. Chen, X. Chen, L. Tang, D. Zhang, Y. Lin, P. Chang, D. Li, Z. Fan, Nano Energy 22 (2016) 539–547.
[28] M. Sharma, P.R. Pudasaini, F. Ruiz-Zepeda, D. Elam, A.A. Ayon, ACS Appl. Mater. Inter. 6 (2014) 4356–4363.
[29] M.M. Adachi, M.P. Anantram, K.S. Karim, Sci. Rep. 3 (2013) 1546.
[30] G. Jia, A. Gawlik, J. Bergmann, B. Eisenhawer, S.S. onherr, G. Andra, F. Falk, IEEE J. Photovolt. 4 (2014) 28–32.
[31] Z. Wang, L. Peng, Z. Lin, J. Ni, P. Yi, X. Lai, X. He, Z. Lei, Sci. Rep. 7 (2017) 13155.
[32] K.Q. Peng, S.T. Lee, Adv. Mater. 23 (2011) 198–215.
[33] J.B.L. Tsakalakos, J. Fronheiser, B.A. Korevaar, O. Sulima, J. Rand, Appl. Phys. Lett. 91 (233113) (2007) 233117.
[34] T.S. Junyi Chen, Wipakorn Jevasuwan, Kotaro Dai, Kei Shinotsuka, Yoshihisa Hatta, Naoki Fukata, Nano Energy 56 (2019) 604–611.
[35] M. Gharghi, E. Fathi, B. Kante, S. Sivoththaman, X. Zhang, Nano Lett. 12 (2012) 6278–6282.
[36] I. Hwang, H.-D. Um, B.-S. Kim, M. Wober, K. Seo, Energy Environ. Sci. 11 (2018) 641–647.
[37] L. Yu, F. Fortuna, B. O'Donnell, G. Patriache, P. Roca i Cabarrocas, Appl. Phys. Lett. 98 (2011) 123113.
[38] L. Yu, F. Fortuna, B. O'Donnell, T. Jeon, M. Foldyna, G. Picardi, P. Roca i Cabarrocas, Nano Lett. 12 (2012) 4153–4158.
[39] S. Misra, L. Yu, M. Foldyna, P. Roca i Cabarrocas, Sol. Energy Mater. Sol. Cells 118 (2013) 90–95.
[40] L. Yu, B. O'Donnell, P.J. Alet, S. Conesa-Boj, F. Peiro, J. Arbiol, P.R. Cabarrocas, Nanotechnology 20 (2009) 225604.
[41] I. Zardo, L. Yu, S. Conesa-Boj, S. Estrade, P.J. Alet, J. Rossler, M. Frimmer, I.C. P. Roca, F. Peiro, J. Arbiol, J.R. Morante, I.M.A. Fontcuberta, Nanotechnology 20 (2009) 155602.
[42] S. Misra, L. Yu, M. Foldyna, P.Ri Cabarrocas, IEEE J. Photovolt. 5 (2015) 40–45.
[43] V. Schmidt, J.V. Wittemann, U. Gösele, Chem. Rev. 110 (2010) 361–388.
[44] V. Schmidt, J.V. Wittemann, S. Senz, U. Gösele, Adv. Mater. 21 (2009) 2681–2702.
[45] S. Cottrino, P. Vivies, D. Fabregue, E. Maire, Acta Mater. 81 (2014) 98–110.
[46] O. Keles, M. Dundar, J. Mater. Process. Technol. 186 (2007) 125–137.
[47] K. Sun, F. Liu, J. Huang, C. Yan, N. Song, H. Sun, C. Xue, Y. Zhang, A. Pu, Y. Shen, J.A. Stride, M. Green, X. Hao, Sol. Energy Mater. Sol. Cells 182 (2018) 14–20.
[48] M. Izu, S.R. Ovshinsky, Thin Solid Films 119 (1984) 55–58.
[49] L. Yu, L. Rigutti, M. Tchernycheva, S. Misra, M. Foldyna, G. Picardi, P. Roca, i Cabarrocas, Nanotechnology 24 (2013) 275401.
[50] S. Zhang, T. Zhang, L. Cao, Z. Liu, J. Wang, J. Xu, K. Chen, L. Yu, Opt. Express 27 (2019) 37248–37256.
[51] S. Misra, L. Yu, W. Chen, M. Foldyna, P.Ri Cabarrocas, J. Phys. D: Appl. Phys. 47 (2014) 393001.
[52] T. Zhang, J. Wang, L. Yu, J. Xu, I.C.P. Roca, Nanotechnology 30 (2019) 302001.

[53] L. Yu, B. O'Donnell, M. Foldyna, P. Roca i Cabarrocas, Nanotechnology 23 (2012) 194011.
[54] J. Ding, Y. Zhou, G. Dong, M. Liu, D. Yu, F. Liu, Prog. Photovolt. 26 (2018) 974–980.
[55] H. Cai, D. Zhang, Y. Xue, K. Tao, Sol. Energy Mater. Sol. Cells 93 (2009) 1959–1962.
[56] P.Y. Dave, K.H. Patel, K.V. Chauhan, A.K. Chawla, S.K. Rawal, Procedia Technol. 23 (2016) 328–335.
[57] T.T. Chau, W.J. Bruckard, P.T. Koh, A.V. Nguyen, Adv. Colloid Interface Sci. 150 (2009) 106–115.